科学通报 2019 年 第 64 卷 第 16 期: 1679 ~ 1690
专题: 无机固体功能材料 论 文
《中国科学》杂志社
SCIENCE CHINA PRESS

$Ca_9Zn_{4.5-\delta}Sb_9(0<\delta<0.5)$化合物Sr/Eu阳离子掺杂与热电性质

张建†, 吴震†, 夏盛清*

山东大学晶体材料研究所国家重点实验室, 济南 250100

† 同等贡献

* 联系人, E-mail: shqxia@sdu.edu.cn

2018-11-29 收稿, 2018-12-30 修回, 2019-01-04 接受, 2019-02-22 网络版发表

国家自然科学基金(51771105)资助

摘要 作为一种非常有前景的热电材料, $Ca_9Zn_{4.5-\delta}Sb_9(0<\delta<0.5)$相较于其他材料有着成本低、环保高效等优势. 以往研究表明间隙金属元素在该体系中起着关键作用, 然而由于其狭窄的域值范围制约了$Ca_9Zn_{4.5-\delta}Sb_9$的性质调控. 本文用原子半径更大的阳离子Sr/Eu来取代少量Ca, 使其Seebeck系数和电学性质得以同步增强, 得到了间接调控间隙原子的结果. 载流子测试表明, 载流子浓度有轻微降低, 而载流子迁移率有着明显提升, 这与增大的晶体热导性质都表明晶体结构发生了明显变化. 对$Ca_{9-x}Sr_xZn_{4.5-\delta}Sb_9(0<\delta<0.5)$系列进行了单晶X射线衍射测试, 结果表明随Sr含量增大晶格参数有增大趋势, 间隙Zn原子浓度上升, 材料热电性能得到协同优化. 最终掺杂样品中, $Ca_{8.2}Eu_{0.8}Zn_{4.5-\delta}Sb_9$在873 K得到最大热电优值($ZT$)约为0.81.

关键词 热电材料, 阳离子, 掺杂, 晶体结构, 尺寸效应

热电材料由于能将自然界废热能源转化为电能继续利用, 一定程度上成为目前能源短缺和环境污染新的解决办法. 但是现在制约其得到广泛应用的主要原因是转化效率太低, 一般只能达到10%左右. 转化效率的优劣是根据无量纲的热电优值(ZT)的大小来判断, $ZT=(\alpha^2T)/(\rho\kappa)$, 其中$\alpha$为Seebeck系数, T为温度, ρ为电阻率, κ为热导率. 式中的各参数都与载流子浓度相关联, 因此热电性能的优化需要考虑各参数的相互影响制约. 在已有的各种体系中, 由于电子和声子传输性质容易调控, 缺陷工程是已知比较常用的手段[1~4], 在经典的热电体系比如PbTe[5~10], Bi_2Te_3[11~14], $CoSb_3$[15~18]中已经成功实现了这种想法. 而作为另一种比较少提及的方法, $SrIn_4$的研究报道中使用了尺寸效应的调控手段[19].

Zintl相有着复杂的晶体结构和较低热导率的特点, 这使其在高温热电能源发电领域表现出了较高的潜能[19,20]. 在过去的数十年中, 大量Zintl相被研究和扩展出. 例如, $CaAl_2Si_2$同构层状材料由于其载流子迁移率值很大而表现出极好的热电性质[21~23]; 而一维链状化合物$Ca_5Al_2Sb_6$[24~26]和Ca_3AlSb_3[27~29]则由于其结构特性表现出很低的晶格热导率. 另外, 在本课题组[30~33]最近的$Ca_{1-x}Ce_xAg_{1-y}Sb(0<x<1, 0<y<1)$和$Ca_9Zn_{4.5-\delta}Sb_9(0<\delta<0.5)$系列工作中也发现, Zintl相中的缺陷效应在调节热电性质方面也有着至关重要的作用. 在对$Ca_9Zn_{4.5-\delta}Sb_9(0<\delta<0.5)$系列进一步的掺杂改性过程中, 我们发现阳离子掺杂样品中存在的尺寸效应, 能得到与缺陷调控工程相似的改性结果.

根据上述所知, 由于其中复杂的晶体结构以及存在的大量过渡金属位置缺陷, $Ca_9Zn_{4.5-\delta}Sb_9(0<\delta<0.5)$系

引用格式: 张建, 吴震, 夏盛清. $Ca_9Zn_{4.5-\delta}Sb_9(0<\delta<0.5)$化合物Sr/Eu阳离子掺杂与热电性质. 科学通报, 2019, 64: 1679–1690
Zhang J, Wu Z, Xia S Q. Sr/Eu cation doping and thermoelectric properties of the compound $Ca_9Zn_{4.5-\delta}Sb_9$ ($0<\delta<0.5$) (in Chinese). Chin Sci Bull, 2019, 64: 1679–1690, doi: 10.1360/N972018-01178

© 2019《中国科学》杂志社

列Zintl相有着不错的热电性质. 已经报道的同系列$Yb_9Mn_{4.2}Sb_9$[34,35], $Eu_9Cd_4Sb_9$[36,37]和$Ca_9Zn_{4.5-x}Cu_xSb_9$[33]化合物材料中取得的最大ZT值可以达到0.7. 最近报道的一篇$Ca_9Zn_{4.5-\delta}Sb_9$研究中, 通过第二相固溶的方法改变了化合物中化学势能进而改变了化合物成分, 增大了过渡金属Zn的含量, 最终在875 K得到了1.1的ZT值[38]. 虽然Zn含量的改变过于微小无法通过测试表征, 但是显著增强的热电性质能够证明过渡金属Zn元素的重要作用.

本文通过阳离子位置Sr, Eu元素的掺杂, 预期通过同样的机理达到调节ZT值的结果. 单晶测试结果表明, 大尺寸元素(Sr, Eu相较于Ca)的掺杂能够使晶体结构c轴方向变大, $Ca_9Zn_{4.5-\delta}Sb_9$($0<\delta<0.5$)中Zn含量计量比没有发生可以检测级别的变化, 但是热电性质能够得到很明显的改善. 在前面已有工作中, 掺杂元素的尺寸效应对材料中载流子浓度的影响在$A_9TM_4Pn_9$(A=碱土金属或二价稀土金属; TM=Zn, Cd; Pn = Sb, Bi)体系中进行研究, 即拥有较大阴离子和较小阳离子尺寸都更容易得到较高的载流子浓度[39]. 因此, 基于这个机理测试中得到的减小的载流子浓度和增大的晶格热导率都是合理的. 通常来讲, Seebeck系数的增大是伴随着电导率的降低, 但在这个体系中Seebeck系数与电导率随掺杂浓度的提高同时存在增大的趋势, 这使得$Ca_9Zn_{4.5}Sb_9$中热电性质得到很大提升. 特别在掺杂比例$Ca_{8.2}Eu_{0.8}Zn_{4.5}Sb_9$中ZT值在873 K下达到了0.81, 这是目前9-4-9相材料中所取得最高数值.

1 实验

(ⅰ) 合成. 单晶合成均在O_2<0.1 ppm(高纯氩气氛中, 0.1 ppm=1.65×10^{-3} mg/L)手套箱中进行, 材料选用Ca(Alfa, 99%), Zn(Alfa, 99.99%), Sb(Alfa, 99.999%), Eu (Alfa, 99.9%), Sr(Alfa, 99%). 将反应物放入Al_2O_3坩埚, 封入石英管进行真空抽滤, 放入马弗炉烧结. 反应在6 h内升温至1175 K, 保温24 h. 反应完成, 以6 K/h降温至873 K, 退火5 h, 10 K/h降至573 K, 保温10 h, 反应结束关闭马弗炉. 将石英管取出, 通风橱内取出反应物, 挑取单晶进行衍射测定.

粉末合成均在手套箱(手套箱氧探头显示0.1 ppm以下)中进行, 材料选用为Ca(Alfa, 99%), Zn(Alfa, 99.99%), Sb(Alfa, 99.999%), Eu(Alfa, 99.9%), Sr(Alfa, 99%). 将反应物封装进Nb管, 然后放入石英管进行真空抽滤, 放入马弗炉烧结. 反应首先在6 h内升温至1173 K, 保温24 h. 反应完成后, 以6 K/h降温速率降至873 K, 退火6 h, 10 K/h速率降至573 K, 反应结束关闭马弗炉. 将合成物在手套箱中打开即可.

(ⅱ) 放电等离子烧结(SPS)实验. 用于热电性质测试的样品都是在型号为SPS1050(Sumitomo Coal Mining Co., Ltd.)仪器上经过SPS进行压制成片. 粉末样品压制前经过XRD测试确保纯度, 而后在手套箱内用研钵磨至均匀细粉, 最后进行SPS压片. 烧结是在973 K下, 加压40 MPa压制7 min, 能够得到致密度在95%以上的样品圆片. 将样品片进行粉末X射线衍射测试表明, 经过SPS后样品无明显第二相出现, 样品有良好稳定性.

(ⅲ) 扫描电子显微镜(SEM). FESEM-4800场发射显微镜(Hitachi), Horiba EX-450能谱仪(EDS), 对样品进行元素测定, 证明了样品中Sr的存在. 测试结果见图S1~S4.

(ⅳ) 单晶X射线衍射仪. 由于该系列晶体在空气中稳定, 因此室温下无需气体保护即可完成下列工艺. 在体视显微镜下选择单晶并切成合适的尺寸, 然后将其安装在石英毛细针的尖端上进行X射线衍射. 数据由装备D8测角仪的Bruker SMART APEX-II CCD检测收集, 该测角仪配备有石墨-单色Mo Kα辐射(λ= 0.71073 Å), 曝光时间为15 s, θ_{max}=28.8°. 通过APEX2软件的INTEGRATE程序进行衍射数据的收集、收敛、积分以及晶胞全球精修. 使用SHELX(版本6.12)程序包进行结构改进, 在精修过程中考虑了原子的各向异性位移参数. 本实验研究中得到$Ca_9Zn_{4.5-\delta}Sb_9$系列化合物的所有晶格常数与之前报道的$Ca_9Zn_{4.5}Sb_9$单晶X射线结构细化(a=21.830(2) Å, b=12.4476(9) Å, c=4.5414(3) Å)中描述的晶格常数一致. 与上面的参数相比, 本文的单胞参数通过粉末X射线衍射所得.

(ⅴ) 粉末X射线衍射仪. 使用具有Cu Kα辐射的Bruker AXS X射线粉末衍射仪在室温下记录粉末X射线衍射图案. 在数据收集期间使用0.02°的步长和10 s的计数时间.

(ⅵ) 热导率. 样品在氩气气氛中使用NETZSCH LFA457仪器进行热导率测试. 使用参比样品为pyroceram 9606($\varnothing$12.7×1.98 mm). 同时测得比热容C_p和热扩散系数D, 样品热导率κ通过$\kappa=C_p\times D\times\rho$计算得到, 其中$\rho$为样品的密度, 测得的温度范围为323~873 K.

(ⅶ) Seebeck系数和电阻率. 在热导率测量之后, 将样品切成具有合适尺寸的长条和方形切片. 长条用

于Seebeck系数和电阻率的测量，并将切片保存在手套箱中以进行霍尔效应测量. 使用Linseis LSR-3/1100仪器系统同时测量样品的Seebeck系数和电阻率，测试温度范围为323~873 K.

(viii) 载流子浓度和迁移率. 在测量之前将尺寸为4 mm×4 mm的正方形样品抛光至约0.5 mm的厚度，并在方片的4个角处镀金作为电极. 使用MMR K2500霍尔效应测试系统在300~573 K的温度范围内测量载流子浓度和迁移率.

2 结果与讨论

2.1 晶体结构

$Ca_9Zn_{4.5-\delta}Sb_9$($0<\delta<0.5$)化合物的阴离子结构由Zn原子与Sb原子构成，相邻的4个$ZnSb_4$四面体通过共顶点连接，在c轴方向上无限延伸形成类一维链状的结构，如图1所示. 在$\delta=0$的化合物中，相邻的Zn_4Sb_9链通过间隙Zn原子相连，进而形成了“准二维层状结构”. δ值由间隙Zn原子浓度决定，并使化合物呈现出较窄的相宽[40]. 并且，间隙Zn原子浓度在$Ca_9Zn_{4.5-\delta}Sb_9$($0<\delta<0.5$)化合物的电输运性质上起着至关重要的作用[33]. 增大间隙原子Zn的浓度可以使载流子迁移率得到极大的提升，并大幅提高材料的电导率；而低浓度间隙Zn原子将导致$Ca_9Zn_{4.5-\delta}Sb_9$($0<\delta<0.5$)表现出较大的电阻值，从而损伤材料的热电性能[22,31,41,42]. 以往的文献[33~38]报道中，主要在9-4-9结构化合物中调节过渡金属间隙原子位置的组成和含量，包括等价元素或者低价元素的掺杂. 本文通过在阳离子位置掺杂大尺寸的阳离子，利用尺寸效应调节晶体结构，以达到提升间隙Zn原子浓度的目的. 虽然间隙Zn原子的微小浓度改变无法通过实验直接表征，但是明显增大的载流子迁移率以及晶格热导率变化均显示这一方法对该系列材料的性能提升有着明显的调控作用. 选用Eu和Sr进行Ca位置的掺杂，制备了$Ca_{9-x}Eu_xZn_{4.5}Sb_9$和$Ca_{9-x}Sr_xZn_{4.5}Sb$(x=0.2，0.4，0.6，0.8)等一系列样品，更高浓度的掺杂出现$EuZn_2Sb_2$和$SrZn_2Sb_2$第二相. 通过粉末X射线衍射测试样品纯度，如图2所示. 结果表明，在Sr/Eu掺杂浓度$x\leqslant0.8$时，样品呈纯相，并且随着掺杂浓度的增大，衍射峰向低角度偏移. 对应(330)衍射峰发生明显偏移，揭示晶体单胞参数沿ab面增大.

为了进一步研究掺杂样品的组成成分，通过高温固相反应生长了不同掺杂浓度的$Ca_{9-x}Sr_xZn_{4.5}Sb_9$单晶，

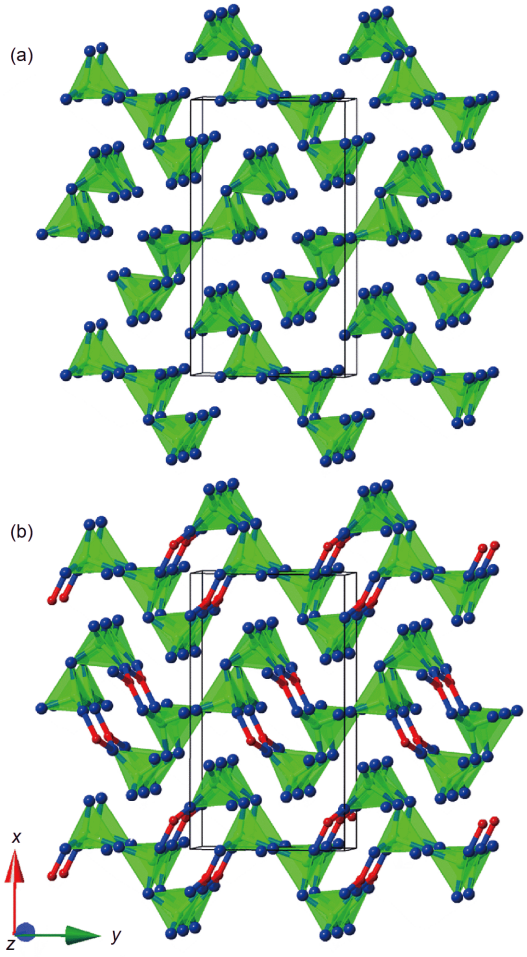


图 1 (网络版彩色)$Ca_9Zn_{4.5-\delta}Sb_9$不同间隙Zn原子占据率晶体结构示意图. (a) δ=0.5, (b) δ=0. 结构中阳离子Ca未显示，Zn和Sb原子分别位于四面体的中心和顶点位置. 间隙Zn原子与相邻的3个四面体顶点相连

Figure 1 (Color online) Side-by-side structure comparison of $Ca_9Zn_{4.5-\delta}Sb_9$ with δ=0.5 (a) and δ=0 (b), viewed along the c axis. The Ca cations are removed for clarity, and the Zn and Sb atoms locate on the tetrahedral centers and vertexes, respectively. The interstitial Zn atoms are linked by three neighboring tetrahedrons

并测试了晶体结构，晶体学数据及结构精修参数等重要单晶衍射数据见表1. 单晶结构所获得最高Sr掺杂浓度对应x=0.58，低于粉末样品x=0.8的掺杂浓度，造成这一差异的原因可能与单晶生长中晶体的质量影响，过高浓度的掺杂比例可能导致单晶质量较差，无法获得可靠晶体数据；其次，掺杂样品可能存在部分偏析情况，导致组分偏离反应计量比(各掺杂样品晶体结构对应的原子坐标、Wyckoff位置、占据率及温度因子参数详见表S1~S4). 尽管如此，系统的单晶结构研究仍带来了一些非常有用的信息. 首先，随着Sr浓度的升高，晶体单胞体积明显增大，主要的晶胞参数变化对应ab

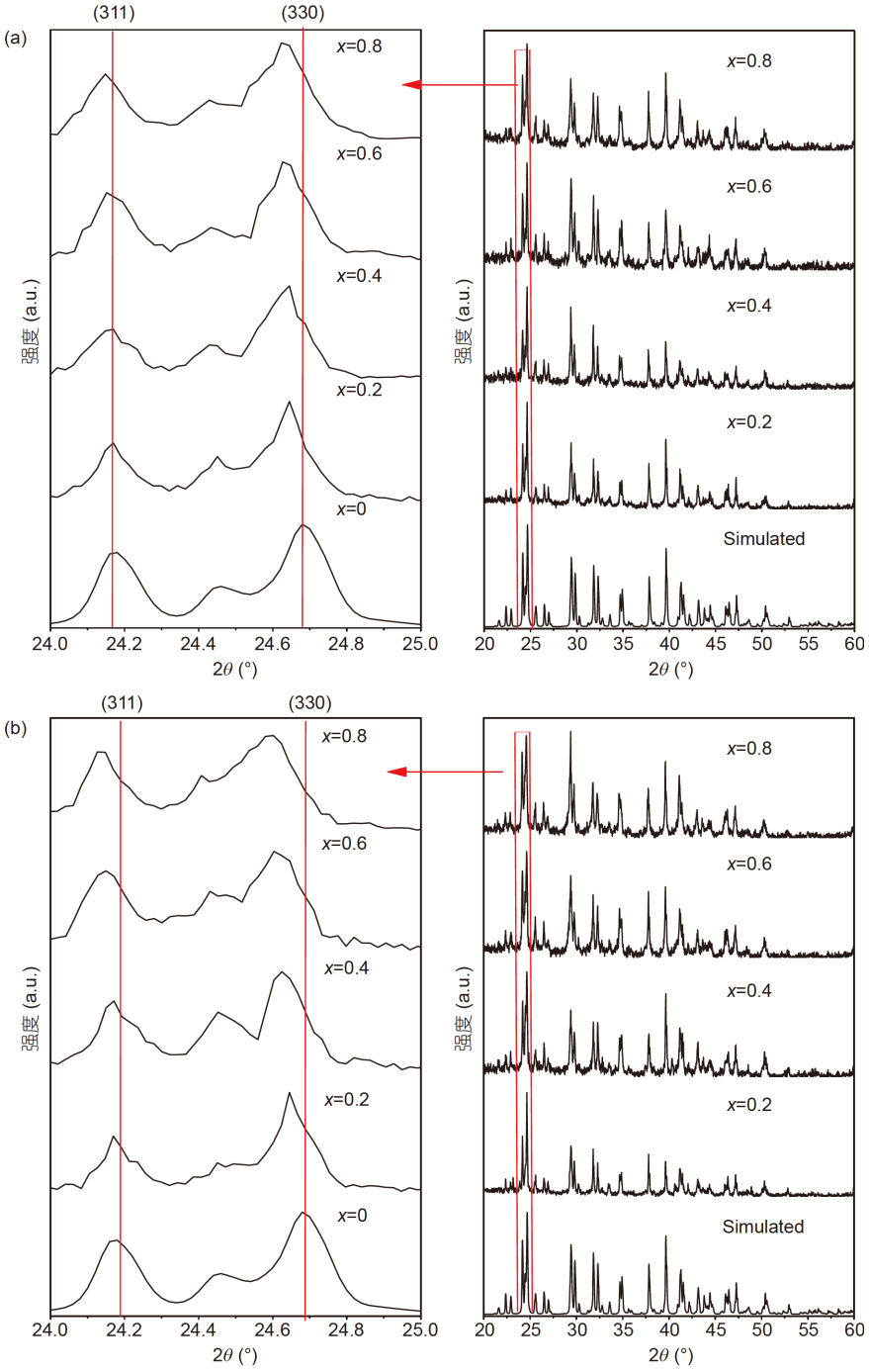


图 2 (网络版彩色)$Ca_{9-x}Eu_xZn_{4.5}Sb_9$(a)及$Ca_{9-x}Sr_xZn_{4.5}Sb_9$(b)(x= 0, 0.2, 0.4, 0.6, 0.8)的粉末衍射图占据率将标准粉末放于图中进行对比. 为了结果更清晰, 右图为截取24°~25°范围与纯相对比衍射峰

Figure 2 (Color online) Powder X-ray diffraction patterns of $Ca_{9-x}Eu_xZn_{4.5}Sb_9$ (a) and $Ca_{9-x}Sr_xZn_{4.5}Sb_9$ (b) (x = 0, 0.2, 0.4, 0.6, 0.8). The simulated pattern is presented for comparison and the diffraction peaks between 24° and 25° is zoomed in for better illustration

平面, 而c轴方向变化不明显, 甚至由于测试的偏差出现数据波动, 这与上述粉末测试结果是一致的. 这说明, 大尺寸的阳离子对$Ca_9Zn_{4.5}Sb_9$掺杂后, 晶格畸变方向优先发生在ab面, 即Zn_4Sb_9链间距离将被拉长, 这一直接的结果将导致间隙原子Zn3的位置产生更大的空间, 理论有利于高浓度的间隙Zn原子. 晶格畸变也体现

表 1 $Ca_{9-x}Sr_xZn_{4.5}Sb_9$样品单晶衍射数据

Table 1 Crystal data and structure refinement for series of $Ca_{9-x}Sr_xZn_{4.5}Sb_9$ samples

分子式	$Ca_{8.42(2)}Sr_{0.58(2)}Zn_{4.47(2)}Sb_9$	$Ca_{8.57(2)}Sr_{0.43(2)}Zn_{4.45(1)}Sb_9$	$Ca_{8.79(2)}Sr_{0.21(2)}Zn_{4.44(1)}Sb_9$	$Ca_9Zn_{4.45(2)}Sb_9$
分子量	1776.01	1767.9	1756.7	1747.69
温度(K)	273(2)	273(2)	273(2)	273(2)
辐射波长	Mo Kα, 0.71073 Å	Mo Kα, 0.71073 Å	Mo Kα, 0.71073 Å	Mo Kα, 0.71073 Å
空间群	*Pbam*(NO.55)	*Pbam*(NO.55)	*Pbam*(NO.55)	*Pbam*(NO.55)
Z	2	2	2	2
a(Å)	12.5563(8)	12.538(4)	12.5185(8)	12.5098(10)
b(Å)	21.9624(13)	21.963(7)	21.9244(13)	21.9023(18)
c(Å)	4.5620(3)	4.5625(14)	4.5571(3)	4.5561(4)
V(Å^3)	1258.05(14)	1256.4(7)	1250.74(14)	1248.34(18)
理论密度(g/cm^3)	4.688	4.673	4.665	4.635
吸收系数(cm^{-1})	1.6571	1.6294	1.5944	1.5508
R_1 [a)]	R_1=0.0378	R_1=0.0316	R_1=0.0341	R_1=0.0350
wR_2 [b)]	wR_2=0.0864	wR_2=0.0628	wR_2=0.0615	wR_2=0.0732
R_{int}	R_1=0.0414	R_1=0.0377	R_1=0.0430	R_1=0.0424
wR_2 [b)]	wR_2=0.0886	wR_2=0.0649	wR_2=0.0639	wR_2=0.0761

a) $R_1=\Sigma||Fo|-|Fc||/\Sigma|Fo|$; b) $wR_2=\Sigma[w(Fo^2-Fc^2)^2]/\Sigma[w(Fo^2)^2]^{1/2}$. 从上至下依次表示: R_1, 对可观察衍射点的R_1值; wR_2, 对可观察衍射点的wR_2值; R_{int}, 对全部衍射点的R_1值; wR_2, 对全部衍射点的wR_2值

于未掺杂样品$Ca_9Zn_{4.45(2)}Sb_9$与Sr掺杂样品$Ca_{8.42(2)}Sr_{0.58(2)}Zn_{4.47(2)}Sb_9$晶体结构中的键长变化, 详见表S5. 由于$Ca_9Zn_{4+x}Sb_9$的特殊结构, 间隙Zn3位置的浓度将略低于理论计量比浓度0.5, 如未掺杂Sr的样品$Ca_9Zn_{4.45(2)}Sb_9$, 经过一系列的掺杂实验, 单晶结构中Zn浓度提升到了$Ca_{8.42(2)}Sr_{0.58(2)}Zn_{4.47(2)}Sb_9$. 虽然这一提升在数值上看似微乎其微, 但是对电输运性质的影响可能是非常明显的. 目前来说, 由于$Ca_9Zn_{4+x}Sb_9$间隙Zn原子浓度的测试尚无准确的方法, 本文的结果首次从实验上证实了间隙Zn原子浓度可精细调控, 这对该体系材料的热电性能研究具有重要的意义.

2.2 载流子浓度和迁移率

霍尔测试在温度区间300~573 K进行, 数据结果如图3所示. 未掺杂的$Ca_9Zn_{4.5}Sb_9$空穴浓度约为2×10^{20} cm^{-3}, 随着Sr/Eu掺杂浓度的上升, 载流子浓度逐渐呈下降趋势, 如$Ca_{8.2}Eu_{0.8}Zn_{4.5}Sb_9$掺杂样品中降至$1.3\times10^{20}$ cm^{-3}. 由于掺杂原子的尺寸效应导致Zintl相化合物的载流子浓度变化已在$Eu_{11}Cd_{6-x}Zn_xSb_{12}$中报道[43], 但与本文报道的$Ca_{9-x}Eu_xZn_{4.5}Sb_9$和$Ca_{9-x}Sr_xZn_{4.5}Sb_9$材料显然有着明显的不同. 正如上述材料晶体结构研究结果显示, 掺杂原子Sr浓度的提升, 可以精细调控p型$Ca_{9-x}Sr_xZn_{4.5}Sb_9$材料中间隙Zn原子浓度, 并间接导致Zn浓度的上升, 而Zn浓度的上升会增加体系的价电子浓度, 进而使费米能级向价带边移动并获得更低的空穴浓度.

虽然晶体结构解析表明Zn含量的增加细微, 但是Sr/Eu掺杂后载流子迁移率的变化特征明显, 这也和我们以前的研究结果一致, 即增加间隙Zn原子的浓度, 可以大幅度提升材料的迁移率, 得益于晶体结构由链状向二维层状的转变[33]. 通常掺杂大尺寸的原子一般会削弱载流子迁移率, 但是霍尔系数测试反而呈现出增强效应, 如在323 K下, $Ca_{8.2}Eu_{0.8}Zn_{4.5}Sb_9$和$Ca_{8.2}Sr_{0.8}Zn_{4.5}Sb_9$的迁移率与未掺杂$Ca_9Zn_{4.5}Sb_9$相比, 由原来的7 cm^2/(V s)分别提升到30和34 cm^2/(V s). 这一结果显然无法用简单的尺寸效应解释, 而应当归结于尺寸效应导致的间隙Zn原子浓度提升. 当然, 这一解释还需要进一步的理论验证, 但是间隙Zn原子浓度的上升会大幅度提升材料的电输运性能并增强材料的热电性能已被前期实验所验证.

2.3 Seebeck系数和电阻率

$Ca_{9-x}Eu_xZn_{4.5}Sb_9$和$Ca_{9-x}Sr_xZn_{4.5}Sb_9$的电阻率和Seebeck系数测试结果如图4所示, 两种掺杂原子均导致材

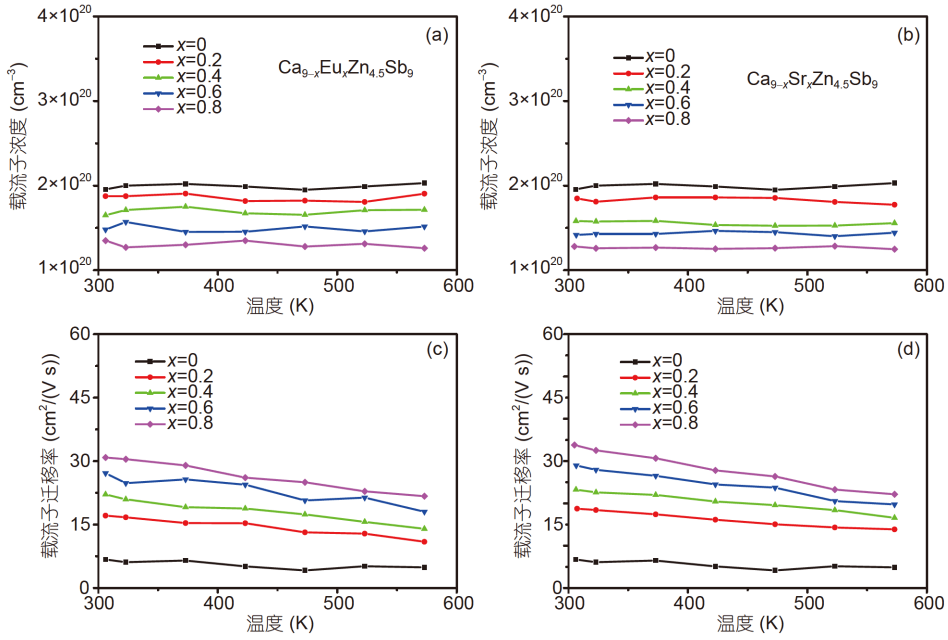


图 3 (网络版彩色)$Ca_{9-x}Eu_xZn_{4.5}Sb_9$(a, c)和$Ca_{9-x}Sr_xZn_{4.5}Sb_9$(b, d)(x=0, 0.2,0.4,0.6,0.8)载流子浓度及迁移率

Figure 3 (Color online) Carrier concentration and mobility of $Ca_{9-x}Eu_xZn_{4.5}Sb_9$ (a, c) and $Ca_{9-x}Sr_xZn_{4.5}Sb_9$ (b, d) (x=0, 0.2, 0.4, 0.6, 0.8)

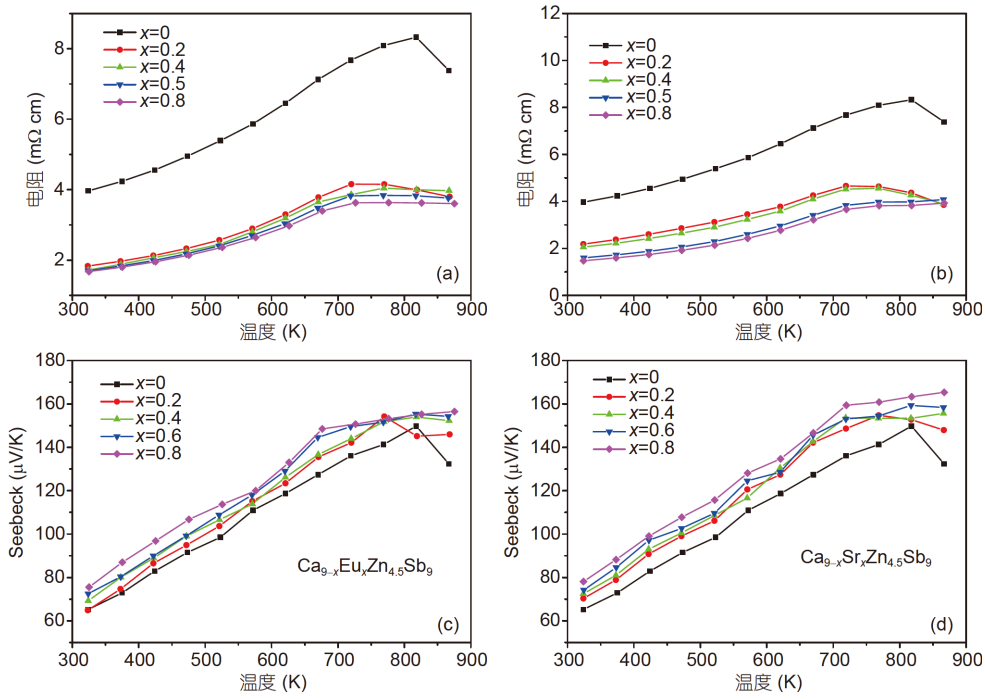


图 4 (网络版彩色)$Ca_{9-x}Eu_xZn_{4.5}Sb_9$(a, c)和$Ca_{9-x}Sr_xZn_{4.5}Sb_9$(b, d)的(x= 0, 0.2, 0.4, 0.6, 0.8)电阻率及Seebeck系数

Figure 4 (Color online) Resistivity and Seebeck coefficient of $Ca_{9-x}Eu_xZn_{4.5}Sb_9$ (a, c) and $Ca_{9-x}Sr_xZn_{4.5}Sb_9$ (b, d) (x = 0, 0.2, 0.4, 0.6, 0.8)

料电阻率显著降低. 理论上而言, Sr比Ca具有更强的给电子能力, Sr替换Ca会导致材料带隙的增大, 并提升材料的电阻率. 但是得益于掺杂后迁移率的增强, 虽然空穴浓度由于带隙的增大略微降低, 但最终材料的导电性被增强. 虽然电阻测试与霍尔系数测试采用不同的设备, 但是二者得到了非常一致的结果, 也进一步证实

了$Ca_9Zn_{4.5}Sb_9$通过大尺寸的Sr/Eu掺杂后，材料的迁移率可以被显著改善. 室温下，未掺杂$Ca_9Zn_{4.5-\delta}Sb_9$的电阻率约在4.0 mΩ cm, 当Eu和Sr掺杂浓度x = 0.2时电阻率降低到1.8 和2.0 mΩ cm. 但是随着Eu或Sr含量的不断增加, 电阻率的变化相对较小, 这是由于Sr/Eu掺杂同时也导致载流子浓度的降低，对电阻率的降低产生负面效应. 随着温度上升, $Ca_{9-x}Eu_xZn_{4.5}Sb_9$和$Ca_{9-x}Sr_xZn_{4.5}Sb_9$的电阻率缓慢上升，在723 K达到最大值. 电阻随温度增大主要原因是载流子浓度基本随温度恒定，但迁移率呈现明显下降趋势，这在9-4-9系列Zintl相化合物中是比较常见的[33~35,37,38]. 随着温度的升高，掺杂后材料的Seebeck系数均呈上升趋势，到700 K达到峰值，这与电阻率变化趋势吻合. 根据经验公式$E_g=2\times\alpha\times T_{max}$, 其中$\alpha$和$T_{max}$分别代表掺杂半导体Seebeck系数峰值及其对应温度. 计算材料所得带隙约是0.25 eV，与文献[33]报道一致. 该系列材料中获得的最大Seebeck系数来自样品$Ca_{0.82}Sr_{0.08}Zn_{4.5}Sb_9$, 数值为165 μV/K, Eu掺杂Seebeck系数相对略低，如$Ca_{0.82}Eu_{0.08}Zn_{4.5-\delta}Sb_9$中最大Seebeck系数为160 μV/K. 值得注意的是，Sr/Eu掺杂使得$Ca_9Zn_{4.5}Sb_9$材料的Seebeck峰值有向低温移动，根据上述能带计算经验公式，T_{max}的减小表明意味着材料的带隙变小，这与经验规律是不符的. 通常而言，同构化合物掺杂电正性更强的同价阳离子，带隙应该增大而不是减小. 这一反常的结果说明，Sr/Eu掺杂可能引起材料的晶体结构改变，例如间隙Zn原子占据率的变化很可能对费米能级附近的能带结构产生影响，甚至导致带隙减小.

为了更好理解掺杂对该系列材料电输运性质的影响，通过SPB模型拟合了有效质量与Seebeck系数的Pisarenko曲线，结果如图5所示. 在323 K时，$Ca_9Zn_{4.5}Sb_9$的Seebeck系数为64 μV/K，通过Sr/Eu掺杂均有明显的提升($Ca_{8.2}Eu_{0.8}Zn_{4.5}Sb_9$, 76 μV/K; $Ca_{8.2}Sr_{0.8}Zn_{4.5}Sb_9$, 79 μV/K). 然而，从单带模型拟合出的Seebeck Pisarenko图表现出明显的多带特征，进一步验证上述推测，Sr/Eu掺杂在材料$Ca_{9-x}Eu_xZn_{4.5}Sb_9$和$Ca_{9-x}Sr_xZn_{4.5}Sb_9$中不仅起着给电子体的作用，而且对能带结构会产生调节作用，这一调节的机制应该来自于间隙Zn原子浓度的变化. 综上所述结果，$Ca_9Zn_{4.5}Sb_9$中采用Sr/Eu掺杂，可以对电传输性质产生协同调控作用，虽然空穴浓度略微减小，但是显著提升的迁移率仍然导致电阻率的明显降低；同时，由于空穴浓度的降低对Seebeck系数具有增强效应，因此Sr/Eu掺杂可以同时提升$Ca_9Zn_{4.5}Sb_9$的Seebeck系数和电导率，这一调控机制在热电材料中是非常有趣的.

2.4 热导率

材料的热导率通常可以分为晶格热导率κ_L和电子热导率κ_e. κ_e可以根据Wiedemann Franz进行计算, $\kappa_e=L\times\sigma\times T$($L$, 洛伦兹常数; σ, 电导率; T, 温度), L可以根据下面公式进行计算, r = −0.5[44~46]:

$$L=\left(\frac{k_B}{e}\right)^2\left(\frac{(r+7/2)F_{r+5/2}(\eta)}{(r+3/2)F_{r+1/2}(\eta)}-\left[\frac{(r+5/2)F_{r+3/2}(\eta)}{(r+3/2)F_{r+1/2}(\eta)}\right]^2\right), \quad (1)$$

$$S=\pm\frac{k_B}{e}\left(\frac{(r+5/2)F_{r+3/2}(\eta)}{(r+3/2)F_{r+1/2}(\eta)}-\eta\right), \quad (2)$$

$$F_n(\eta)=\int_0^\infty\frac{x^n}{1+e^{x-\eta}}dx. \quad (3)$$

$Ca_{9-x}Eu_xZn_{4.5}Sb_9$和$Ca_{9-x}Sr_xZn_{4.5}Sb_9$计算所得电子热导率及晶格热导率如图6所示. 随着Sr/Eu浓度的增大，由于电导率的提升电子热导率有着同步的提升. 同样晶格热导率也随着掺杂浓度的增大而增大，这一结果也不能用经验规律来理解. 通常阳离子位置掺杂更

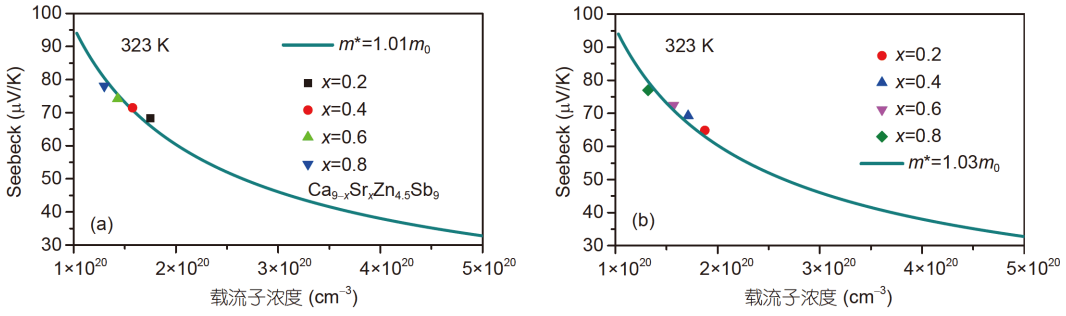


图 5 (网络版彩色)在323 K时, 根据SPB模型计算得出的Pisarenko曲线. (a) $Ca_{9-x}Eu_xZn_{4.5}Sb_9$, (b) $Ca_{9-x}Sr_xZn_{4.5}Sb_9$. x= 0, 0.2, 0.4, 0.6, 0.8

Figure 5 (Color online) Seebeck Pisarenko plot of $Ca_{9-x}Sr_xZn_{4.5}Sb_9$ (a) and $Ca_{9-x}Eu_xZn_{4.5}Sb_9$ (b). x = 0, 0.2, 0.4, 0.6, 0.8

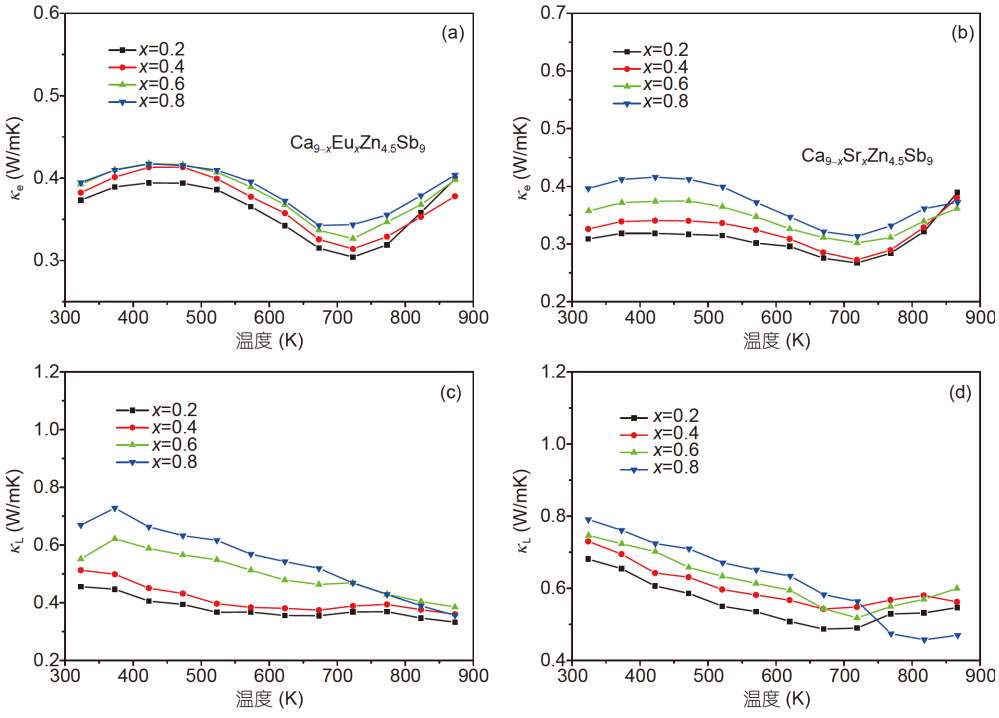


图 6 (网络版彩色)$Ca_{9-x}Eu_xZn_{4.5}Sb_9$(a, c)和$Ca_{9-x}Sr_xZn_{4.5}Sb_9$(b, d)(x= 0, 0.2, 0.4, 0.6, 0.8)电子热导率κ_e及晶格热导率κ_L

Figure 6 (Color online) Electronic and lattice components of thermal conductivity for $Ca_{9-x}Eu_xZn_{4.5}Sb_9$ ((a), (c)) and $Ca_{9-x}Sr_xZn_{4.5}Sb_9$ ((b), (d)) (x= 0, 0.2, 0.4, 0.6, 0.8)

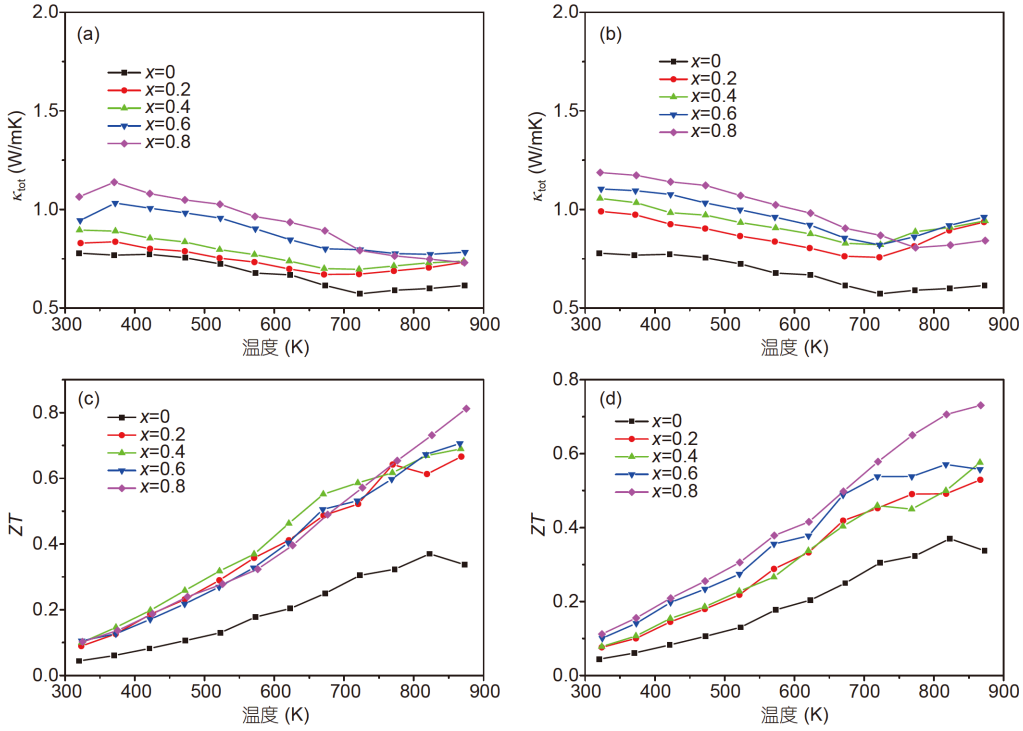


图 7 (网络版彩色)$Ca_{9-x}Eu_xZn_{4.5}Sb_9$((a), (c))和$Ca_{9-x}Sr_xZn_{4.5}Sb_9$((b), (d))(x= 0, 0.2, 0.4, 0.6, 0.8)总热导率κ_{tot}及热电优值ZT

Figure 7 (Color online) Thermal conductivity and calculated figure of merit for materials $Ca_{9-x}Eu_xZn_{4.5}Sb_9$ (a), (c) and $Ca_{9-x}Sr_xZn_{4.5}Sb_9$ (b), (d) (x=0, 0.2, 0.4, 0.6, 0.8)

重的原子后，由于晶格有序度的破坏和重原子本身的原因，对应的晶格热导率应该降低，因此$Ca_{9-x}Eu_xZn_{4.5}Sb_9$和$Ca_{9-x}Sr_xZn_{4.5}Sb_9$中的晶格热导率增大现象从另一面说明了Sr/Eu掺杂对应着晶体结构的细微改变. 正如单晶解析数据表明, 对应的间隙Zn原子浓度增大, 链状结构进一步向层状结构转化，这对材料的晶格热导率提升是有促进作用的.

尽管Sr/Eu掺杂促使了材料$Ca_9Zn_{4.5}Sb_9$总热导率的提升, 但是由于其本身复杂的晶体结构, 热导率仍维持在较低的水平，如图7所示. 在室温下，掺杂浓度x对应的0~0.8区间内，$Ca_{9-x}Eu_xZn_{4.5}Sb_9$从0.77增大到1.06 W/(m K)，而$Ca_{9-x}Sr_xZn_{4.5}Sb_9$则增大到1.22 W/(m K). 当温度低于723 K时, 热导率随温度增大而减小; 高于723 K则由于双极效应使得热导明显提升. 由于Sr/Eu掺杂对电功系数的明显增大作用，所得的材料热电优值均表现出明显的增强, 特别是$Ca_{8.2}Eu_{0.8}Zn_{4.5}Sb_9$在873 K获得到最大$ZT$~0.81，这也是目前在9-4-9单相热电材料中实验获得的最佳数据.

3 总结

通过采用大尺寸阳离子Sr/Eu对材料$Ca_9Zn_{4.5-\delta}Sb_9$进行掺杂, 可以大幅度提升材料的热电性能. 虽然相关的掺杂机制十分复杂, 并且得到很多反常的结果, 但是各项实验数据均指向材料中的间隙Zn原子浓度增大, 这一调控机制显然与传统的热电材料掺杂调节作用不同. Sr/Eu掺杂后$Ca_9Zn_{4.5-\delta}Sb_9$热电性能的优化应归结于内部缺陷结构的改变，间隙Zn原子浓度提升后晶体结构由一维链状向二维层状结构的转化，这一结构变化可以协同提升材料的电导率和Seebeck系数. 由于9-4-9系列化合物中固有的相宽较窄，以往的实验结果在如何有效提升其间隙原子浓度方面均未给出较为有效的手段，因此本文的结果对该系列材料的热电性质调控具有重要的意义，并且这一特殊的调控机制对于其他热电材料的改性研究可能也具有一定的帮助.

参考文献

1 Zhu T, Liu Y, Fu C, et al. Compromise and synergy in high-efficiency thermoelectric materials. Adv Mater, 2017, 29: 1605884
2 Li Z, Xiao C, Zhu H, et al. Defect chemistry for thermoelectric materials. J Am Chem Soc, 2016, 138: 14810–14819
3 Xiao C, Li Z, Li K, et al. Decoupling interrelated parameters for designing high performance thermoelectric materials. Acc Chem Res, 2014, 47: 1287–1295
4 Pei Y, Shi X, LaLonde A, et al. Convergence of electronic bands for high performance bulk thermoelectrics. Nature, 2011, 473: 66–69
5 Heremans J P, Jovovic V, Toberer E S, et al. Enhancement of thermoelectric efficiency in PbTe by distortion of the electronic density of states. Science, 2008, 321: 554–557
6 Pei Y, LaLonde A, Iwanaga S, et al. High thermoelectric figure of merit in heavy hole dominated PbTe. Energy Environ Sci, 2011, 4: 2085–2089
7 Wang H, Pei Y, LaLonde A D, et al. Heavily doped p-type PbSe with high thermoelectric performance: An alternative for PbTe. Adv Mater, 2011, 23: 1366–1370
8 Li W, Zheng L, Ge B, et al. Promoting SnTe as an eco-friendly solution for p-PbTe thermoelectric via band convergence and interstitial defects. Adv Mater, 2017, 29: 1605887
9 Takagiwa Y, Pei Y, Pomrehn G, et al. Validity of rigid band approximation of PbTe thermoelectric materials. APL Mater, 2013, 1: 011101
10 Wang H, Gibbs Z M, Takagiwa Y, et al. Tuning bands of PbSe for better thermoelectric efficiency. Energy Environ Sci, 2014, 7: 804–811
11 Hu L, Wu H, Zhu T, et al. Tuning multiscale microstructures to enhance thermoelectric performance of n-type bismuth-telluride-based solid solutions. Adv Energy Mater, 2015, 5: 1500411
12 Devender, Gehring P, Gaul A, et al. Harnessing topological band effects in bismuth telluride selenide for large enhancements in thermoelectric properties through isovalent doping. Adv Mater, 2016, 28: 6436–6441
13 Hu L P, Zhu T J, Wang Y G, et al. Shifting up the optimum figure of merit of p-type bismuth telluride-based thermoelectric materials for power generation by suppressing intrinsic conduction. NPG Asia Mater, 2014, 6: e88
14 Hu L, Zhu T, Liu X, et al. Point Defect engineering of high-performance bismuth-telluride-based thermoelectric materials. Adv Funct Mater, 2014, 24: 5211–5218
15 Li G, Aydemir U, Wood M, et al. Defect-controlled electronic structure and phase stability in thermoelectric skutterudite $CoSb_3$. Chem Mater, 2017, 29: 3999–4007
16 Li G, Bajaj S, Aydemir U, et al. p-Type co interstitial defects in thermoelectric skutterudite $CoSb_3$ due to the breakage of Sb_4-rings. Chem Mater, 2016, 28: 2172–2179
17 Qiu Y, Xi L, Shi X, et al. Charge-compensated compound defects in Ga-containing thermoelectric skutterudites. Adv Funct Mater, 2013, 23: 3194–

3203
18 Tang Y, Qiu Y, Xi L, et al. Phase diagram of In-Co-Sb system and thermoelectric properties of in-containing skutterudites. Energy Environ Sci, 2014, 7: 812−819
19 Brown S R, Kauzlarich S M, Gascoin F, et al. $Yb_{14}MnSb_{11}$: New high efficiency thermoelectric material for power generation. Chem Mater, 2006, 18: 1873–1877
20 Toberer E S, Cox C A, Brown S R, et al. Traversing the metal-insulator transition in a Zintl phase: Rational enhancement of thermoelectric efficiency in $Yb_{14}Mn_{1-x}Al_xSb_{11}$. Adv Funct Mater, 2008, 18: 2795–2800
21 Gascoin F, Ottensmann S, Stark D, et al. Zintl phases as thermoelectric materials: Tuned transport properties of the compounds $Ca_xYb_{1-x}Zn_2Sb_2$. Adv Funct Mater, 2005, 15: 1860–1864
22 Shuai J, Liu Z, Kim H S, et al. Thermoelectric properties of Bi-based Zintl compounds $Ca_{1-x}Yb_xMg_2Bi_2$. J Mater Chem A, 2016, 4: 4312–4320
23 Zhang J, Song L, Madsen G K H, et al. Designing high-performance layered thermoelectric materials through orbital engineering. Nat Commun, 2016, 7: 10892
24 Zevalkink A, Toberer E S, Bleith T, et al. Improved carrier concentration control in Zn-doped $Ca_5Al_2Sb_6$. J Appl Phys, 2011, 110: 013721
25 Zevalkink A, Swallow J, Snyder G J. Thermoelectric properties of Zn-doped $Ca_5In_2Sb_6$. Dalton Trans, 2013, 42: 9713–9719
26 Toberer E S, Zevalkink A, Crisosto N, et al. The Zintl compound $Ca_5Al_2Sb_6$ for low-cost thermoelectric power generation. Adv Funct Mater, 2010, 20: 4375–4380
27 Zevalkink A, Toberer E S, Zeier W G, et al. Ca_3AlSb_3: An inexpensive, non-toxic thermoelectric material for waste heat recovery. Energy Environ Sci, 2011, 4: 510–518
28 Zevalkink A, Zeier W G, Pomrehn G, et al. Thermoelectric properties of Sr_3GaSb_3 – A chain-forming Zintl compound. Energy Environ Sci, 2012, 5: 9121–9128
29 Shi Q, Feng Z, Yan Y, et al. Electronic structure and thermoelectric properties of Zintl compounds A_3AlSb_3 (A=Ca and Sr): First-principles study. RSC Adv, 2015, 5: 65133–65138
30 Pomrehn G S, Zevalkink A, Zeier W G, et al. Defect-controlled electronic properties in AZn_2Sb_2 Zintl phases. Angew Chem Int Ed, 2014, 53: 3422–3426
31 Zevalkink A, Zeier W G, Cheng E, et al. Nonstoichiometry in the Zintl phase $Yb_{1-\delta}Zn_2Sb_2$ as a route to thermoelectric optimization. Chem Mater, 2014, 26: 5710–5717
32 Wang J, Liu X C, Xia S Q, et al. $Ca_{1-x}RE_xAg_{1-y}Sb$ (RE=La, Ce, Pr, Nd, Sm$0\leqslant x\leqslant 1$; $0\leqslant y\leqslant 1$): Interesting structural transformation and enhanced high-temperature thermoelectric performance. J Am Chem Soc, 2013, 135: 11840–11848
33 Wu Z, Li J, Li X, et al. Tuning the thermoelectric properties of $Ca_9Zn_{4+x}Sb_9$ by controlled doping on the interstitial structure. Chem Mater, 2016, 28: 6917–6924
34 Bux S K, Zevalkink A, Janka O, et al. Glass-like lattice thermal conductivity and high thermoelectric efficiency in $Yb_9Mn_{4.2}Sb_9$. J Mater Chem A, 2014, 2: 215–220
35 Ohno S, Zevalkink A, Takagiwa Y, et al. Thermoelectric properties of the $Yb_9Mn_{4.2-x}Zn_xSb_9$ solid solutions. J Mater Chem A, 2014, 2: 7478–7483
36 Kazem N, Hurtado A, Klobes B, et al. $Eu_9Cd_{4-x}CM_{2+x-y}\square_ySb_9$:$Ca_9Mn_4Bi_9$-type structure stuffed with coinage metals (Cu, Ag, and Au) and the challenges with classical valence theory in describing these possible Zintl phases. Inorg Chem, 2015, 54: 850–859
37 Kazem N, Zaikina J V, Ohno S, et al. Coinage-metal-stuffed $Eu_9Cd_4Sb_9$: Metallic compounds with anomalous low thermal conductivities. Chem Mater, 2015, 27: 7508–7519
38 Ohno S, Aydemir U, Amsler M, et al. Achieving $zT>1$ in inexpensive Zintl phase $Ca_9Zn_{4+x}Sb_9$ by phase boundary mapping. Adv Funct Mater, 2017, 27: 1606361
39 Xia S, Bobev S. Interplay between size and electronic effects in determining the homogeneity range of the $A_9Zn_{4+x}Pn_9$ and $A_9Cd_{4+x}Pn_9$ Phases ($0\leqslant x\leqslant 0.5$), A=Ca, Sr, Yb, Eu; Pn=Sb, Bi. J Am Chem Soc, 2007, 129: 10011–10018
40 Bobev S, Thompson J D, Sarrao J L, et al. Probing the limits of the Zintl concept: Structure and bonding in rare-earth and alkaline-earth zinc-antimonides $Yb_9Zn_{4+x}Sb_9$ and $Ca_9Zn_{4.5}Sb_9$. Inorg Chem, 2004, 43: 5044–5052
41 Shuai J, Geng H Y, Lan Y C, et al. Higher thermoelectric performance of Zintl phases $Eu_{0.5}Yb_{0.51-x}Ca_xMg_2Bi_2$ by band engineering and strain fluctuation. Proc Natl Acad Sci USA, 2016, 113: E4125−E4132
42 Tamaki H, Sato H K, Kanno T. Isotropic conduction network and defect chemistry in $Mg_{3+\delta}Sb_2$-based layered Zintl compounds with high thermoelectric performance. Adv Mater, 2016, 28: 10182–10187
43 Pauling L. The Nature of the Chemical Bond. New York: Cornell University Press, 1960. 88−93
44 Jonson M, Mahan G D. Mott's formula for the thermopower and the Wiedemann-Franz law. Phys Rev B, 1980, 21: 4223–4229
45 Kumar G S, Prasad G, Pohl R O. Experimental determinations of the Lorenz number. J Mater Sci, 1993, 28: 4261–4272

46 Zhao L D, Lo S H, He J, et al. High performance thermoelectrics from earth-abundant materials: Enhanced figure of merit in PbS by second phase nanostructures. J Am Chem Soc, 2011, 133: 20476–20487

补充材料

图S1 $Ca_9Zn_{4.45(2)}Sb_9$ EDS数据
图S2 $Ca_{8.79(2)}Sr_{0.21(2)}Zn_{4.44(1)}Sb_9$ EDS数据
图S3 $Ca_{8.57(2)}Sr_{0.43(2)}Zn_{4.45(1)}Sb_9$ EDS数据
图S4 $Ca_{8.42(2)}Sr_{0.58(2)}Zn_{4.47(2)}Sb_9$ EDS数据
表S1 $Ca_9Zn_{4.45(2)}Sb_9$原子坐标、Wyckoff位置、占据率及温度因子等参数
表S2 $Ca_{8.79(2)}Sr_{0.21(2)}Zn_{4.44(1)}Sb_9$原子坐标、Wyckoff位置、占据率及温度因子等参数
表S3 $Ca_{8.57(2)}Sr_{0.43(2)}Zn_{4.45(1)}Sb_9$原子坐标、Wyckoff位置、占据率及温度因子等参数
表S4 $Ca_{8.42(2)}Sr_{0.58(2)}Zn_{4.47(2)}Sb_9$原子坐标、Wyckoff位置、占据率及温度因子等参数
表S5 $Ca_9Zn_{4.45(2)}Sb_9$和$Ca_{8.42(2)}Sr_{0.58(2)}Zn_{4.47(2)}Sb_9$的部分键长

本文以上补充材料见网络版csb.scichina.com. 补充材料为作者提供的原始数据, 作者对其学术质量和内容负责.

Summary for "$Ca_9Zn_{4.5-\delta}Sb_9$($0<\delta<0.5$)化合物Sr/Eu阳离子掺杂与热电性质"

Sr/Eu cation doping and thermoelectric properties of the compound $Ca_9Zn_{4.5-\delta}Sb_9$ ($0<\delta<0.5$)

Jian Zhang[†], Zhen Wu[†] & Shengqing Xia[*]

State Key Laboratory of Crystal Materials, Institute of Crystal Materials, Shandong University, Jinan 250100, China
† These authors contributed equally to this work
* Corresponding author, Email: shqxia@sdu.edu.cn

Previous studies suggested that Zintl phases related to the $Ca_9Zn_{4.5-\delta}Sb_9$ ($0<\delta<0.5$) structure may be very promising thermoelectric candidates because of the complex crystal structure and extensively existing transition metal defects. Studies on compounds $Yb_9Mn_{4.2}Sb_9$, $Eu_9Cd_4Sb_9$ and $Ca_9Zn_{4.5-x}Cu_xSb_9$ indicated that they could achieve an optimized zT around 0.7. Especially for $Ca_9Zn_{4.5-\delta}Sb_9$, a very recent report suggested that a high zT of 1.1 at 875 K could be obtained in combination of various secondary phases introduced by the variation of Zn contents, which provided a chemical potential to change the composition. However, to change the composition of $Ca_9Zn_{4.5-\delta}Sb_9$ is actually very difficult to implement owing to the narrow homogeneity range. In this work, with Ca substituted by big cations such as Eu^{2+} and Sr^{2+}, the unit cell of $Ca_9Zn_{4.5-\delta}Sb_9$ was expanded, and similar significant enhancement on the thermoelectric performance was resulted.

All syntheses were handled inside a glovebox, then the reactants were loaded in the Nb tube and arc-welded, which were enclosed in a fused silica tube. The reactions were firstly heated to 1173 K in 6 h and then maintained at this temperature for 24 h. After the homogeneity process, the furnace was slowly cooled down to 873 K at a rate of 6 K/h, followed by another dwelling for 6 hours and finally cooled down to 573 K at a rate of 10 K/h. At last, the furnace was shut down and the reactions were opened in the glovebox. The compound were fully characterized by single-crystal X-ray diffraction (SXRD) and powder X-ray diffraction(PXRD), Energy dispersive spectrometer (EDS) and Hall effect measurement, etc. Single-crystal X-ray diffraction (SXRD) proves that with the increase of Sr component, the crystal parameters are slightly increasing. Hall effect measurement show that the substitution of Ca by Eu or Sr can both lead to an obvious decreasing on the carrier (holes) concentration, and the resultant mobility for Sr/Eu-doped materials is very similar if compared by the same doping level. It is also noted that neither the carrier concentration nor the mobility seems to vary linearly with the Eu/Sr-doping contents, which means a saturated state will be eventually approached. This phenomenon is consistent with the speculation above that the changes on the properties should predominantly originate from the change of interstitial Zn content, which the size effect dominated. While the decreasing carrier concentrations as well as the increasing mobility and lattice thermal conductivity all point to a structure modification, the crystal structures of these doped materials were systematically verified through the single crystal X-ray diffraction.

In conclusion, although a direct measurement on such a small composition variation is very difficult (the X-ray diffraction results prove it), the significantly reduced carrier concentration and increased mobility as well as lattice thermal conductivity can still provide some useful hints on understanding the property optimization of these materials. For material $Ca_{8.2}Eu_{0.8}Zn_{4.5-\delta}Sb_9$, high figure of merit with ZT~0.81 has been achieved at 873 K.

Zintl phases, thermoelectric materials, defects, crystal structures, interstitials

doi: 10.1360/N972018-01178